Solid-State Electronics 71 (2012) 25–29

Contents lists available at SciVerse ScienceDirect

Solid-State Electronics

journal homepage: www.elsevier.com/locate/sse

Temperature dependence of the transport properties of spin field-effect transistors built with InAs and Si channels

D. Osintsev *, V. Sverdlov, Z. Stanojević, A. Makarov, S. Selberherr

Institute for Microelectronics, TU Wien Gußhausstraße 27-29, A-1040 Wien, Austria

ARTICLE INFO

Article history:
Available online 2 January 2012

Keywords:
Spin field-effect transistor
Dresselhaus spin–orbit interaction
Tunneling magnetoresistance
Conductance
Temperature
Current

ABSTRACT

We study the transport properties of the Datta–Das spin field-effect transistor built on InAs and Si. First, we demonstrate that the amplitude of the magnetoresistance oscillations as a function of the band mismatch between the ferromagnetic contacts and the semiconductor channel made of InAs decreases dramatically with increasing temperature. A shorter InAs channel is needed to create an InAs-based SpinFET which will operate at higher temperatures. Second, we show that the [100] orientation of the fin is preferable for silicon SpinFETs due to stronger modulation of the conductance as a function of spin–orbit interaction and magnetic field. Short silicon fins can be used for current modulation as a function of the conduction band mismatch between the channel and the ferromagnetic contacts only at relatively low temperatures. In contrast, longer silicon channels allow a TMR modulation at room temperature by changing the strength of the spin–orbit interaction through the gate bias.

© 2011 Elsevier Ltd. All rights reserved.

1. Introduction

Utilizing spin properties of electrons for future microelectronic devices opens great opportunities to reduce device power consumption. In recent years spintronic devices, where the spin of the electron is used as additional degree of freedom to tune their properties, have received much attention. The spin field-effect transistor (SpinFET) is a future semiconductor spintronic device promising to deliver a performance superior to that achieved with present transistor technology. SpinFETs are composed of two ferromagnetic contacts (source and drain), which sandwich the semiconductor region. Ferromagnetic contacts contain mostly spin-polarized electrons and play the role of polarizer and analyzer as described by Datta and Das [1]. The ferromagnetic source contact injects spin-polarized electrons into the semiconductor region. Because of the non-zero spin–orbit interaction the electron spin precesses during the propagation through the channel. At the drain contact only the electrons with spin aligned to the drain magnetization can easily leave the channel and contribute most to the current. Thus, the total current through the device depends on the relative angle between the magnetization direction of the drain contact and the electron spin polarization at the end of the semiconductor channel. Current modulation is achieved by tuning the strength of the spin–orbit interaction in the semiconductor region and thus the degree of the spin precession. Importantly, the strength of the spin–orbit interaction in the channel depends on the effective electric field and can be controlled by the voltage applied to the gate.

The spin precession angle $\Delta\theta$ defined as the difference between the orientation of the spin of the electron at the end and at the beginning of the semiconductor region is [2]

$$\Delta\theta = \frac{2\alpha m^*}{\hbar^2} L, \quad (1)$$

where α is the strength of the spin–orbit interaction, m^* is the effective mass of the electron, $\hbar$ is the reduced Planck constant, and L is the length of the semiconductor channel. In the absence of spin–orbit interaction and external magnetic field the electrons propagate with their spin orientation conserved. The strength of the spin–orbit interaction determines the minimum length of the semiconductor channel, which will be sufficient to change the orientation of the spin to opposite. In case of a material with a strong spin–orbit interaction such as InAs the semiconductor channel will be shorter than for a material with the weaker spin–orbit interaction such as silicon.

The spin–orbit coupling is usually taken in the Rashba form [3], with the corresponding effective Hamiltonian

$$H_R = \frac{\alpha_R}{\hbar}(p_x\sigma_y - p_y\sigma_x), \quad (2)$$

where α_R is the effective electric field-dependent parameter of the spin–orbit interaction, p_x and p_y are the electron momentum projections, σ_x and σ_y are the Pauli matrices. The Rashba form of the

* Corresponding author.
E-mail addresses: osintsev@iue.tuwien.ac.at (D. Osintsev), sverdlov@iue.tuwien.ac.at (V. Sverdlov), stanojevic@iue.tuwien.ac.at (Z. Stanojević), makarov@iue.tuwien.ac.at (A. Makarov), selberherr@iue.tuwien.ac.at (S. Selberherr).

0038-1101/$ - see front matter © 2011 Elsevier Ltd. All rights reserved.
doi:10.1016/j.sse.2011.10.015

spin–orbit coupling will be used when analyzing transport properties in InAs channels in §3.1 below.

Silicon is characterized by a weak spin–orbit interaction and, as a consequence, it has a long spin life time. It is therefore an attractive material for spin current propagation. However, because of its weak spin–orbit interaction, silicon was not considered as a candidate for the SpinFET channel material. Recently, however, it was shown [4] that thin silicon films inside SiGe/Si/SiGe structures may have relatively large values of spin–orbit interaction. Interestingly, the strength of the Rashba spin–orbit interaction is relatively small and is approximately ten times smaller than the value of the dominant contribution which is of the Dresselhaus type with a corresponding effective Hamiltonian in the form

$$H_D = \frac{\beta}{\hbar}(p_x\sigma_x - p_y\sigma_y). \tag{3}$$

This major contribution to the spin–orbit interaction is due to interfacial disorder induced inversion symmetry breaking and depends almost linearly on the effective electric field [5]. For a built-in field of 50 kV/cm, the strength of the Dresselhaus spin–orbit interaction is found to be $\beta \approx 2$ μeV nm, which is in agreement with the value found experimentally [6], while $\alpha_R \approx 0.1$ μeV nm. This value of the spin–orbit interaction in confined silicon systems is sufficient for their applications as SpinFET channels.

The stronger spin–orbit interaction leads to an increased spin relaxation. The Dyakonov–Perel mechanism is the main spin relaxation mechanism in systems, where the electron dispersion curves for the two spin projections are non-degenerate. In quasi-one-dimensional electron structures, however, a suppression of this spin relaxation mechanism is expected [7]. Indeed, in case of elastic scattering only back-scattering is allowed. Reversal of the electron momentum results in the inversion of the effective magnetic field direction. Therefore, the precession angle does not depend on the number of scattering events along the carrier trajectory in the channel, but is a function of the channel length alone. Thus, the spin-independent elastic scattering does not result in additional spin decoherence. In the presence of an external magnetic field, however, spin-flip processes become possible, and the Elliott–Yafet spin relaxation mechanism is likely relevant [8].

2. Model

To calculate the transport properties of a ballistic spin field-effect transistor we consider a model similar to [8,9]. The Hamiltonian in the ferromagnetic regions has the following form in the one-band effective mass approximation

$$\widehat{H}_F^L = \frac{\hat{p}_x^2}{2m_f^*} + h_0\hat{\sigma}_z, \quad x < 0, \tag{4}$$

$$\widehat{H}_F^R = \frac{\hat{p}_x^2}{2m_f^*} \pm h_0\hat{\sigma}_z, \quad x > L, \tag{5}$$

where m_f^* is the effective mass in the contacts, $h_0 = 2PE_F/(P^2+1)$ is the exchange splitting energy with P defined as the spin polarization in the ferromagnetic regions, E_F is the Fermi energy, and $\hat{\sigma}_z$ is the Pauli matrix; ± in (5) stands for the parallel and anti-parallel configuration of the contact magnetization. For the semiconductor channel region the Hamiltonian reads [8,9]

$$\widehat{H}_S = \frac{\hat{p}_x^2}{2m_s^*} + \delta E_c - \frac{\alpha_R}{\hbar}\hat{\sigma}_y\hat{p}_x + \frac{1}{2}g\mu_B B\hat{\sigma}^*, \tag{6}$$

where m_s^* is the subband effective mass, δE_c is the band mismatch between the ferromagnetic and the semiconductor region, α_R is the strength of the spin–orbit interaction, g is the Landé factor, μ_B is the Bohr magneton, B is the magnetic field, and $\hat{\sigma}^* \equiv \hat{\sigma}_x\cos\gamma + \hat{\sigma}_y\sin\gamma$ with γ defined as the angle between the magnetic field and the transport direction.

To calculate the dependence of the transport properties on the spin–orbit interaction we need the electron eigenfunctions in the various regions. For the ferromagnetic regions spin-up and spin-down eigenstates have the form $(1,0)^\dagger$ and $(0,1)^\dagger$, respectively. The wave function in the left contact has the following form [8,9]

$$\Psi_{L\uparrow}(x) = (e^{ik_\uparrow x} + R_\uparrow e^{-ik_\uparrow x})\begin{pmatrix}1\\0\end{pmatrix} + R_\downarrow e^{-ik_\downarrow x}\begin{pmatrix}0\\1\end{pmatrix}, \tag{7}$$

$$\Psi_{L\downarrow}(x) = R_\uparrow e^{-ik_\uparrow x}\begin{pmatrix}1\\0\end{pmatrix} + (e^{ik_\downarrow x} + R_\downarrow e^{-ik_\downarrow x})\begin{pmatrix}0\\1\end{pmatrix}, \tag{8}$$

where (7) represents the incoming spin-up electrons and (8) the incoming spin-down electrons, correspondingly, $k_{\uparrow(\downarrow)} = \sqrt{2m_f^*(E \mp h_0)/\hbar^2}$ is the wave vector of the spin-up (spin-down) electron and $R_{\uparrow(\downarrow)}$ is the amplitude of the reflected wave. For the right contact the wave function is given by [8,9]

$$\Psi_R(x) = C_\uparrow e^{ik_\uparrow x}\begin{pmatrix}1\\0\end{pmatrix} + C_\downarrow e^{ik_\downarrow x}\begin{pmatrix}0\\1\end{pmatrix}. \tag{9}$$

For the semiconductor region the wave function can be written as [8,9]

$$\Psi_S(x) = A_+ e^{ik_{x1}^{(+)}x}\begin{pmatrix}k_1\\1\end{pmatrix} + B_+ e^{ik_{x2}^{(+)}x}\begin{pmatrix}k_2\\1\end{pmatrix} + A_- e^{ik_{x1}^{(-)}x}\begin{pmatrix}k_3\\-1\end{pmatrix} + B_- e^{ik_{x2}^{(-)}x}\begin{pmatrix}k_4\\-1,\end{pmatrix} \tag{10}$$

where $k_{x1(x2)}^{(+)}$ and $k_{x1(x2)}^{(-)}$ are the wave vectors obtained by solving the equations $\frac{\hbar^2k^2}{2m_s^*} + \delta E_c \pm \sqrt{\left(\frac{Bg\mu_B\cos(\gamma)}{2}\right)^2 + \left(\frac{Bg\mu_B\sin(\gamma)}{2} - \alpha_R k\right)^2} = E$, respectively. The coefficients k_1, k_2, k_3, k_4 are calculated as [8,9]

$$k_1 = -\frac{i\left(Bg\mu_B\sin(\gamma) - 2\alpha_R k_{x1}^{(+)}\right) - Bg\mu_B\cos(\gamma)}{2\sqrt{\left(\frac{Bg\mu_B\cos(\gamma)}{2}\right)^2 + \left(\frac{Bg\mu_B\sin(\gamma)}{2} - \alpha_R k_{x1}^{(+)}\right)^2}}, \tag{11}$$

$$k_2 = -\frac{i\left(Bg\mu_B\sin(\gamma) - 2\alpha_R k_{x2}^{(+)}\right) - Bg\mu_B\cos(\gamma)}{2\sqrt{\left(\frac{Bg\mu_B\cos(\gamma)}{2}\right)^2 + \left(\frac{Bg\mu_B\sin(\gamma)}{2} - \alpha_R k_{x2}^{(+)}\right)^2}}, \tag{12}$$

$$k_3 = \frac{i\left(Bg\mu_B\sin(\gamma) - 2\alpha_R k_{x1}^{(-)}\right) - Bg\mu_B\cos(\gamma)}{2\sqrt{\left(\frac{Bg\mu_B\cos(\gamma)}{2}\right)^2 + \left(\frac{Bg\mu_B\sin(\gamma)}{2} - \alpha_R k_{x1}^{(-)}\right)^2}}, \tag{13}$$

$$k_4 = \frac{i\left(Bg\mu_B\sin(\gamma) - 2\alpha_R k_{x2}^{(-)}\right) - Bg\mu_B\cos(\gamma)}{2\sqrt{\left(\frac{Bg\mu_B\cos(\gamma)}{2}\right)^2 + \left(\frac{Bg\mu_B\sin(\gamma)}{2} - \alpha_R k_{x2}^{(-)}\right)^2}}. \tag{14}$$

The reflection and transmission coefficients are determined by applying the boundary conditions at the ferromagnet/semiconductor interfaces.

We compute the current through the device as [14,15]

$$I^{P(AP)}(V) = \frac{e}{h} \times \int_{\delta E}^{\infty} \left[T_\uparrow^{P(AP)}(E) + T_\downarrow^{P(AP)}(E)\right]\left\{\frac{1}{1+e^{\frac{E-E_F}{k_BT}}} - \frac{1}{1+e^{\frac{E-E_F+eV}{k_BT}}}\right\} dE, \tag{15}$$

where k_B is the Boltzmann constant, T is the temperature, and V is the voltage. The spin-up $\left(T_\uparrow^P\right)$ and spin-down $\left(T_\downarrow^P\right)$ transmission probabilities for the parallel configuration of the contact magnetization are defined as

$$T_{\uparrow}^{P} = |C_{\uparrow}|^2 + \frac{k_{\downarrow}}{k_{\uparrow}}|C_{\downarrow}|^2, \tag{16}$$

$$T_{\downarrow}^{P} = \frac{k_{\uparrow}}{k_{\downarrow}}|C_{\uparrow}|^2 + |C_{\downarrow}|^2. \tag{17}$$

For the anti-parallel configuration of the contact magnetization the transmission probabilities are given by

$$T_{\uparrow}^{AP} = \frac{k_{\downarrow}}{k_{\uparrow}}|C_{\uparrow}|^2 + |C_{\downarrow}|^2, \tag{18}$$

$$T_{\downarrow}^{AP} = |C_{\uparrow}|^2 + \frac{k_{\uparrow}}{k_{\downarrow}}|C_{\downarrow}|^2. \tag{19}$$

The conductance is defined as

$$G^{P(AP)} = \lim_{V\to 0} \frac{I^{P(AP)}}{V}. \tag{20}$$

In the limit of low temperature the conductance must coincide with the one obtained from the Laudauer–Büttiker formula [15,16]

$$G^{P(AP)} = \frac{e^2}{h}\left(T_{\uparrow}^{P(AP)}(E_F) + T_{\downarrow}^{P(AP)}(E_F)\right). \tag{21}$$

Finally, the tunneling magnetoresistance (TMR) is defined as [8,9]

$$\mathrm{TMR} \equiv \frac{G^{P} - G^{AP}}{G^{AP}}. \tag{22}$$

3. Results and discussion

In our calculations we use two types of material for the semiconductor region: InAs, which is characterized by a strong value of the spin–orbit interaction, and silicon, which is characterized by a moderate value of the spin–orbit interaction.

3.1. InAs channels

For all calculations for the InAs semiconductor channel we assume the dominant mechanism of the spin–orbit coupling is due to the geometry-induced inversion symmetry breaking (Rashba type). Common simulation parameters are as follows: the effective mass for the ferromagnetic region $m_f^* = m_0$ and for the semiconductor region $m_s^* = 0.036\ m_0$, where m_0 is the electron rest mass. Fig. 1 shows the dependence of the TMR on the value of the band mismatch δE_c between the ferromagnetic source contact and the semiconductor channel. The TMR oscillates between positive and negative values. As the length of the semiconductor channel decreases, the period of the oscillations increases roughly proportionally to the inverse length of the semiconductor channel.

Temperature exerts a significant influence on the device characteristics as shown in Fig. 2. For a channel length $L = 0.05$ μm the oscillatory amplitude of the TMR decreases for $T = 77$ K and completely vanishes for $T = 180$ K. The reason for the oscillatory behavior to disappear at $T = 180$ K is a relatively short period of the conductance oscillations (and correspondingly TMR oscillation shown in Fig. 1) with respect to δE_c. Thus one can expect that for the shorter channel the amplitude of oscillations is sufficient to modulate the current in the SpinFET at higher temperatures.

To facilitate the injection of the spin-polarized current into the channel we introduce, following [8] and [9], delta-function barriers of strength $z = 2m_f^* U/\hbar^2 k_F$, where $k_F = \sqrt{2m_f^* E_F/\hbar^2}$, at the interfaces between the contacts and the channel. The current dependence on the value of the drain-source voltage is shown in Fig. 3. A clear S-like shape of the curves is observed at $T = 10$ K. This is a manifestation of the conductance oscillations as a function of δE_c, which have a large amplitude due to the presence of the delta-function barriers at the interfaces between the contact and the channel ($z = 3$). A large amplitude of the conductance oscillations guarantees the different slopes of the IV curves corresponding to different δE_c. Although the S-like non-linearity is not well pronounced at higher temperatures, the difference in the slopes at small voltages is not completely washed out, even at room temperature.

3.2. Silicon channels

We consider square silicon fins with [1 0 0] or [1 1 0] orientation, with (0 0 1) horizontal faces. The parabolic band approximation for the band structure in silicon is not sufficient to accurately obtain the subband structure in thin and narrow silicon fins. We employ the two-band $\mathbf{k}\cdot\mathbf{p}$ model proposed in [10], which has been shown to be accurate up to 0.5 eV above the conduction band edge in silicon [11]. The resulting Schrödinger differential equation, with the confinement potential appropriately added to the Hamiltonian [10], is discretized using the box integration method and solved for each value of the conserved momentum p_x along the current direction using efficient numerical algorithms available through the Vienna Schrödinger-Poisson framework (VSP) [12].

Fig. 4 demonstrates the dependence of the subband minima as function of the fin thickness t for the lowest four subbands; the fin orientation is along the [1 1 0] direction. The dependence of the splitting between the unprimed subbands with decreasing t, which are perfectly degenerate in the effective mass approximation, is

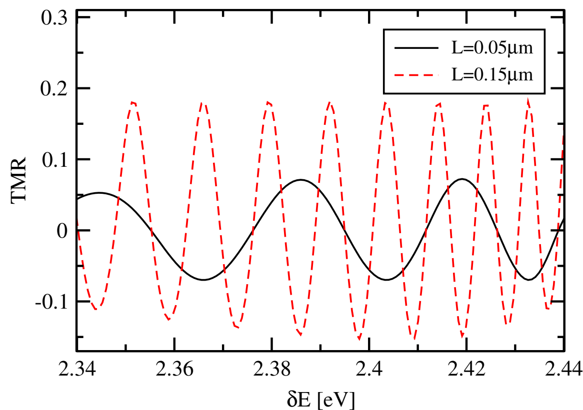

Fig. 1. TMR dependence on the value of δE_c, for $E_F = 2.47$ eV, $P = 0.4$, $B = 0$T, $z = 0$, $\alpha_R = 42.3$ meV nm, $T = 0$ K.

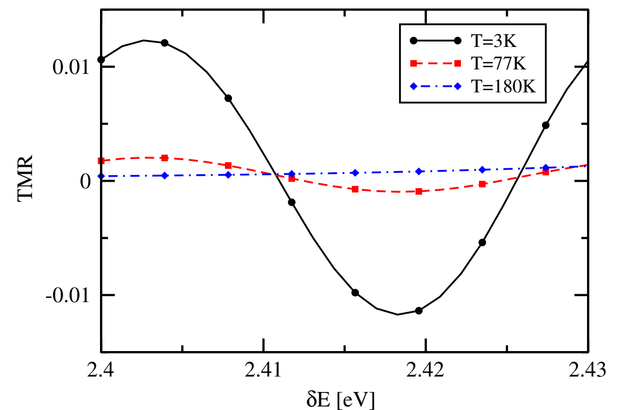

Fig. 2. TMR dependence on the value of δE_c, for $\alpha_R = 31.7$meV nm, $E_F = 2.47$ eV, $P = 0.4$, $B = 0$T, $z = 0$, $L = 0.05$ μm.

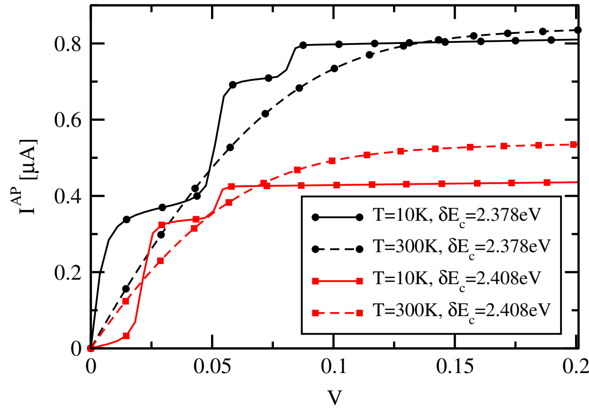

Fig. 3. Current dependence on the value of the drain-source voltage for $B=$ 0T, $z=$ 3, $L=$ 0.03 μm, $P=$ 0.4.

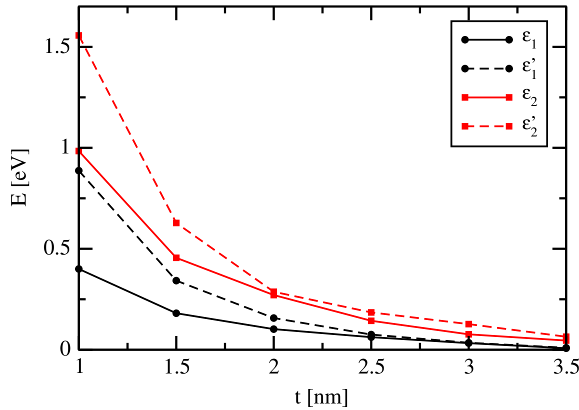

Fig. 4. Subband minima as a function of thickness t in a [110]-oriented fin.

clearly seen. Splitting between valleys in a [100] fin is negligible [13]. In contrast to that, the dependence of the effective mass of the ground subband in [100] fins on t is more pronounced as compared to [110] fins. Results of density-functional calculations [13] confirm the mass dependences obtained from the $\mathbf{k}\cdot\mathbf{p}$ model (Fig. 5).

With the values of the effective masses and subband offsets obtained, we study the conductance properties for the parallel and anti-parallel configurations of the contact magnetization. The

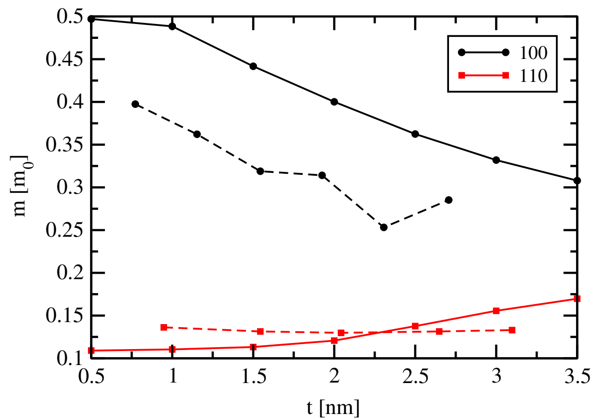

Fig. 5. Ground subband effective mass dependence on t in [100] and [110] fins. Open symbols are from [13].

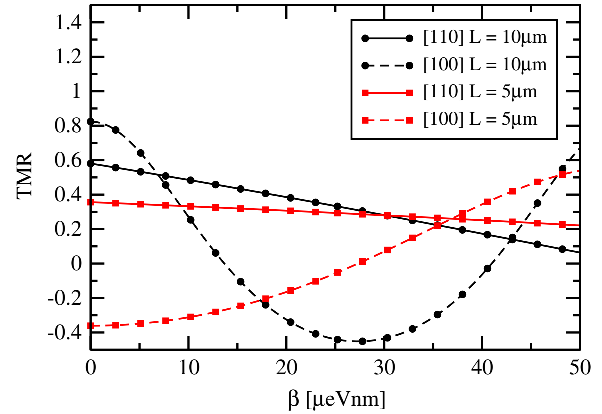

Fig. 6. TMR dependence on the value of the Dresselhaus spin–orbit interaction for $t=$ 1.5 nm, $B=$ 4T, $P=$ 0.6, $z=$ 3, $\gamma=$ 0, $T=$ 0 K.

spin–orbit interaction is treated in the Dresselhaus form Eq. (3). The Hamiltonian in the channel for [100] oriented fins reads

$$\widehat{H}_S=\sum_n \frac{\hat{p}_x^2}{2m_n^*}+\delta E_n-\frac{\beta}{\hbar}\hat{\sigma}_x\hat{p}_x+\frac{1}{2}g\mu_B B\hat{\sigma}^*, \qquad (23)$$

and

$$\widehat{H}_S=\sum_n \frac{\hat{p}_x^2}{2m_n^*}+\delta E_n-\frac{\beta}{\hbar}\hat{\sigma}_y\hat{p}_x+\frac{1}{2}g\mu_B B\hat{\sigma}^*, \qquad (24)$$

for [110] oriented fins. Here m_n^* is the subband effective mass, δE_n is the subband mismatch between the ferromagnetic region and the channel, and β is the strength of the spin–orbit interaction.

Fig. 6 shows the dependence of the TMR for [100] and [110] oriented fins with $t=1.5$ nm on the value of the spin–orbit interaction. Fins with [100] orientation show a stronger dependence on β compared to [110] oriented fins. Thus [100] oriented fins are preferred for silicon SpinFETs. The reason of the stronger dependence is that the characteristic length on which the spin–orbit interaction produces the full spin precession is defined by the inverse of the wave vector $k_D=m_n^*\beta/\hbar^2$. As shown in Fig. 5, the effective mass value for the [110] oriented fins is smaller compared to the [100] oriented fins, hence for the same variation of k_D in case of the [110] oriented fins a larger variation of β is required to achieve the same TMR value modulation.

Fig. 7 shows the dependence of the oscillations of the TMR on the value of the conduction band mismatch δE_c. The period of the oscillations is roughly inversely proportional to the length of

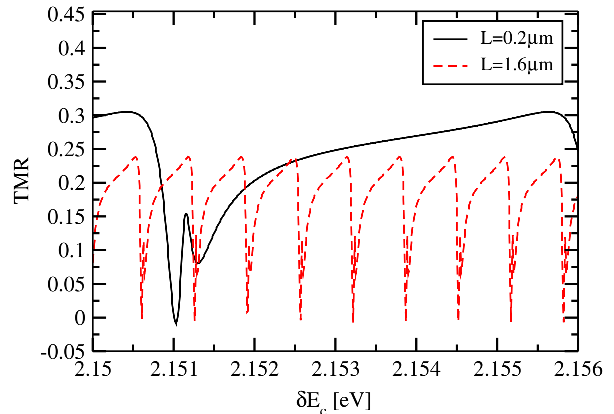

Fig. 7. TMR dependence on the value of the δE_c for $E_F=2.47$ eV, $P=$ 0.4, $z=$ 3, $\beta=42.3$ μeV nm, $T=$ 0 K.

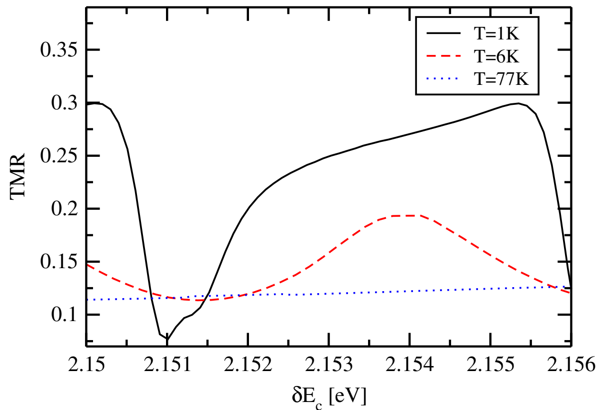

Fig. 8. TMR dependence on the value of the δE_c for E_F = 2.47 eV, P = 0.4, z = 3, L = 0,2μm, V = 0.1 meV, β = 42.3 μeV nm.

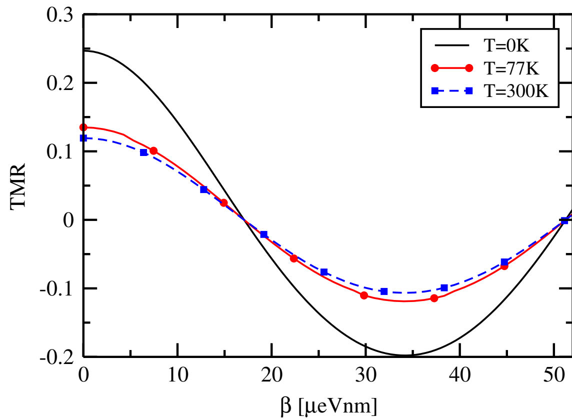

Fig. 9. TMR dependence on the value of the Dresselhaus spin–orbit interaction for E_F = 2.47 eV, δE_c = 2.154 eV, P = 0.4, z = 3, L = 8 μm, V = 1 meV.

the semiconductor channel as also shown in Fig. 1. The presence of the delta-function barriers at the interfaces between the contact and the channel exerts a significant influence on the oscillation shape. For higher and thicker barriers, the TMR, although being a periodic function of the conductance band mismatch, stops oscillating around zero and becomes positive (or negative) in a broad range of the conduction band mismatch. This sign definitiveness leads to the complete absence of the oscillations of the TMR at T = 77 K as shown in Fig. 8. It is important that, although reduced, the TMR is not zero at 77 K. Therefore, the TMR modulation as a function of the spin–orbit interaction strength is preserved even at high temperatures as shown in Fig. 9. This opens the possibility to modulate the TMR by changing the value of β even at room temperature.

4. Summary and conclusion

A short semiconductor channel length provides a possibility to create an InAs-based SpinFET which will operate at room temperature. Silicon fins of [100] orientation are best suited for silicon-based SpinFETs. Short silicon fins can be used for current modulation as a function of the conduction band mismatch between the channel and the ferromagnetic contacts only at relatively low temperatures. In contrast, longer silicon channels allow a TMR modulation at room temperature by changing the strength of the spin–orbit interaction through the gate bias.

Acknowledgment

This work is supported by the European Research Council through the grant #247056 MOSILSPIN.

References

[1] Datta S, Das B. Electronic analog of the electro-optic modulator. Appl Phys Lett 1990;56(7):665–7.
[2] Sugahara S, Nitta J. Spin-transistor electronics: an overview and outlook. In: Proceedings of the IEEE, vol. 98(12); 2010.
[3] Giglberger S, Golub LE, Bel'kov VV, Danilov SN, Schuh D, Gerl C, et al. Rashba and dresselhaus spin splittings in semiconductor quantum wells measured by spin photocurrents. Phys Rev B 2007;75(3):035327.
[4] Nestoklon MO, Ivchenko EL, Jancu J-M, Voisin P. Electric field effect on electron spin splitting in SiGe/Si quantum wells. Phys Rev B 2008;77(15):155328.
[5] Prada M, Klimeck G, Joynt R. Spin-orbit splittings in Si/SiGe quantum wells: from ideal Si membranes to realistic heterostructures. New J Phys 2011;13:013009.
[6] Wilamowski Z, Jantsch W. Suppression of spin relaxation of conduction electrons by cyclotron motion. Phys Rev B 2004;69(3):035328.
[7] Bournel A, Dollfus P, Bruno P, Hesto P. Gate-induced spin precession in an $In_{0.53}Ga_{0.47}As$ two dimensional electron gas. European Phys J Appl Phys 1998;4(1):1–4.
[8] Cahay M, Bandyopadhyay S. Phase-coherent quantum mechanical spin transport in a weakly disordered quasi-one-dimensional channel. Phys Rev B 2004;69(4):045303.
[9] Jiang K, Zhang R, Yang J, Yue C-X, Sun Z-Y. Tunneling magnetoresistance properties in ballistic spin field-effect transistors. IEEE Trans. Electron Dev. 2010:2005–12.
[10] Bir GL, Pikus GE. Symmetry and strain-induced effects in semiconductors. Wiley; 1974.
[11] Sverdlov V, Baumgartner O, Windbacher T, Selberherr S. Modeling of modern MOSFETs with strain. J Comput Electron 2009;8:192–208.
[12] Karner M, Gehring A, Holzer S, Pourfath M, Wagner M, Gs W, et al. A multi-purpose Schrödinger-Poisson solver for TCAD applications. J Comput Electron 2007;6:179–82.
[13] Tsuchiya H, Ando H, Sawamoto S, Maegawa T, Hara T, Yao H, et al. Comparisons of performance potentials of silicon nanowire and graphene nanoribbon MOSFETs considering first-principles bandstructure effects. IEEE Trans Electron Dev 2010;57(2):406–14.
[14] Osintsev D, Sverdlov V, Stanojevic Z, Makarov A, Selberherr S. Transport properties of spin field-effect transistors built on Si and InAs, 2011. In: 12th International Conference on Ultimate Integration on Silicon (ULIS); 2011. p. 1–4.
[15] Landauer R. Spatial variation of currents and fields due to localized scatterers in metallic conduction. IBM J Res Dev 1957;1(3):223–31.
[16] Büttiker M. Four-terminal phase-coherent conductance. Phys Rev Lett 1986;57:1761–4.